



Continuous flow microcalorimetry as a tool for studying catalytic hydrogenations: application to CO₂ methanation

Yamily Mateo Rosado¹ · Alain Ledoux¹ · Laurent Balland¹ · Isabelle Polaert¹

Received: 12 July 2023 / Accepted: 13 December 2023 / Published online: 21 January 2024
© Akadémiai Kiadó, Budapest, Hungary 2024

Abstract

A new experimental method for the estimation of kinetic parameters using the signal of the heat flow from a differential scanning calorimeter is presented. An isothermal gas solid reaction was carried out in a differential scanning calorimeter (DSC) in continuous flow on a fixed bed of catalyst in the crucible. An instantaneous energy balance in steady state was made for estimate the total heat flow produced by the reaction and deduce the kinetics parameters. Hydrogenation of CO₂ on Ni/Al₂O₃ solid catalyst was used to produce methane as base reaction. This reaction was chosen because it is very exothermic, and also a well-known reaction in terms of kinetics. A large range of stoichiometric and non-stoichiometric operating conditions were studied with ratios of reactants H₂/CO₂ between 3 and 7, diluted with N₂ at different isothermal conditions in an interval of temperature between 573 and 673 K for different flow rates of mixture of gases. CO₂ methanation involves several reactions in parallel where the main ones are the Sabatier reaction and the reverse water gas shift (RWGS) reaction. To keep the isothermicity of the catalytic bed, a theoretical analysis of heat and mass transfer limitations was carried out to determine the absence of the internal and external limitation in the kinetic data.

Keywords Calorimetry · DSC · Heat-flow · Continuous flow · Kinetics · Estimation of parameters

List of symbols

Ea_i	Activation energy of reaction I (J mol ⁻¹)
F	Molar flow rate (mol s ⁻¹)
f_q	Optimization criterion (–)
$k_{\infty i \text{ PL-1}}$	Kinetic constant–pre-exponential factor PL-1
$k_{\infty i \text{ PL-2}}$	Kinetic constant–pre-exponential factor PL-2
Keq_i	Equilibrium constant of reaction i (–)
m_{cat}	Catalyst mass (g)
n_i	Reaction order PL-1 (–)
o_i	Reaction order PL-2 (–)
P	Pressure (bar)
P_j	Partial pressure of species j (bar)
q	Heat flow (W)
R	Perfect gas constant (J mol ⁻¹ K ⁻¹)
T	Temperature (K)
y_j	Molar fraction of species j (–)
Y_j	Adimensionally flow rates (–)

Greek letters

α_i	Chemical expansion (–)
ν_{ij}	Stoichiometric coefficient(–)
ΔH_i	Enthalpy of reaction i (J mol ⁻¹)
χ_i	Extent of reaction i (–)
r_i	Reaction rate of reaction i (mol g ⁻¹ s ⁻¹)

Subscript

CSTR	Continuously stirred tank reactor
DSC	Differential scanning calorimetry
RWGS	Reverse water gas shift
μGC	Micro gas phase chromatograph

Introduction

The kinetic characterization of chemical processes is fundamental to understand and optimize industrial processes. In complex catalytic reactions, an important experimental phase is necessary that includes the performance of numerous manipulations with various operating conditions to collect the data on which the development of the model will be based, which makes this process more complex and longer. Calorimetry is a valuable tool for rapid determination of kinetic parameters, as it allows measuring the heat flow that

✉ Isabelle Polaert
isabelle.polaert@insa-rouen.fr

¹ LSPC, INSA Rouen Normandie, Univ Rouen Normandie, Normandie Université, UR 4704, F-76000 Rouen, France

occurs during physical and chemical transformations [1]. This technique involves the use of a calorimeter, which is a device that measure the amount of heat exchanged between the system and the surrounding environment and these can be batch or continuous flow reactors [2, 3]. Depending on the configuration of the calorimeter, reaction calorimetry can be divided into four operating modes: adiabatic mode, isoperibolic mode, isothermal mode and scanning mode [4–6].

Microcalorimetry is a specialized branch of calorimetry. This technique measures very small heat changes in small sample volumes. One of the most common microcalorimetric techniques for the study of various simple or complex substances is differential scanning calorimetry (DSC) [7]. It is a thermal analysis technique that measures the difference of heat flow between a sample and a reference material as a function of time or temperature in isothermal or non-isothermal mode as the reactions take place [8]. To improve the sensitivity and resolution of DSC measurements, three-dimensional shape temperature sensor is very useful because they can provide more accurate measurements than traditional flat sensors. This technique uses a group of thermocouples surrounding the sample and allows temperature to be measured with high resolution, allowing for more detailed measurements of heat flow and thermal properties [9].

Differential scanning calorimetry (DSC) is a powerful analytical technique that has gained popularity in recent years due to its ability to provide highly sensitive and accurate thermal analysis data of materials and substances, including the determination of phase transitions, chemical reactions, and changes in heat capacity [2, 10]. For that reason, this technique has aroused interest of researchers from various fields such as polymers (Drzeżdżon et al. [11]), pharmaceuticals (Clas et al. [12]), food (Leyvia-Porras et al. [13]). The heat flow signal measured by a DSC during the reaction allows to estimate the kinetic parameters as shown Pagano et al. [14, 15]. Their estimation procedure is based on the use of an energy balance on the encapsulated sample of epoxy resin in the DSC. A differential–algebraic approach was adopted in their method, making possible the use of direct measurements of the heat rate of reaction released by the DSC. With this approach, good agreement between experimental and predicted data was achieved.

This article proposes a methodology to develop an isothermal model for a heterogeneous (gas–solid) reaction using a continuous flow DSC considering the catalytic crucible as a continuous stirred tank reactor (CSTR). In this method, the reactants are continuously fed, which allows the continuous measurement of heat flow in the system. This is a simple and fast method to estimate the kinetics of the catalytic reaction using a small sample volume. Estimation of kinetics parameters (activation energy, kinetic constant and

reaction order) based on heat flow measurement allows to determine the extent reaction, which reduces the necessity to perform numerous output analyses, making it a very useful tool for optimizing the kinetic modeling stage.

Experimental

Materials

The gases used in this study are carbon dioxide and hydrogen as methanation reagents, and nitrogen as carrier gas. The bottles of gases CO₂, H₂, and N₂ were provided by Linde and they have a high purity of 99.95%. The catalyst used was developed by Alrafi et al. [16], which is based on nickel dispersed on an alumina support (Ni/Al₂O₃). Nickel has a mass composition of 15% and is in the form of a fine powder with diameter < 50 μm. We have chosen this catalyst since it has been used in others studies about CO₂ methanation reaction and also because nickel is the most widely used catalyst owing to its high selectivity in this reaction and low cost [17–20].

Reaction support

We have used the hydrogenation of CO₂ to produce methane as base reaction. We have chosen this reaction because CO₂ hydrogenation is very exothermic, and it is a well-known reaction in terms of kinetics [21], and also because in last years, the global philosophy in research and industry field is to reduce CO₂ emissions to the environment [22]. Many strategies have been developed for this purpose, one of them is hydrogenation of CO₂ to obtain different high value products [23]. CO₂ methanation involves several reactions in parallel where the main ones are:

Sabatier reaction $CO_2 + 4H_2 \rightleftharpoons CH_4 + 2H_2O \Delta H_R = -165.0 \text{ kJ mol}^{-1}$ (**R₁**).

Reverse Water Gas Shift (RWGS) $CO_2 + H_2 \rightleftharpoons CO + H_2O \Delta H_R = 41.2 \text{ kJ mol}^{-1}$ (**R₂**).

Reactor configuration

The SENSYS Evo DSC in continuous flow was used as heat flow measure equipment. This device provides high accuracy ($\pm 0.4\%$ of calorimetric precision) in heat measurements thanks to its “3D” sensor based on thermocouples. The three-dimensional sensor of this device is composed of 2 cylindrical thermopiles composed by 10 rings each containing 12 thermocouples. Every thermopile surrounds the sample or the reference all along the lateral surface of the crucibles.

As our experimental system implements a heterogeneous gas–solid reaction, the cell with catalytic crucible of the DSC is used. For every experiment we have used 0.013 g of catalyst in the measure cell and the same value of mass of Al_2O_3 in the reference cell. The crucibles containing the sample and reference are placed directly in the center of the furnace area, which operates in a temperature range between room temperature and 873 K.

To obtain the measured heat flow from the DSC, the flow rates of gases are first adjusted at room temperature and then cells are heating with a temperature ramp of 4 K min^{-1} up to the setpoint temperature. When the system is finally stabilized, heat flow is continuously recovered. The temperature is increased at the next setpoint temperature and the process is repeated. For the validation of our results, in one of our experiments the output gases were analyzed inline by a CHEMLYS micro gas phase chromatograph (μGC) [24]. Figure 1 shows the schematic representation of the experimental installation. The three inlet gases are regulated by Bronkhorst flowmeter and then mixed through a fitting before entering the DSC. To ensure the passage of the same mixing flow rate in both cells, the series configuration, reference cell then measurement cell, has been used. We show detailed schematic view of the crucible with the gas flow inlet and outlet and the catalyst bed, we can see clearly how the gas flow through the catalyst and how the catalyst is trapped inside the cell.

Model

Hypothesis

Our model considers the crucible containing the catalyst as a continuous stirred tank reactor (CSTR). Therefore, composition, temperature and pressure at outlet are considered the same as inside the reactor, allowing to obtain a system of algebraic equations to be solved, thus facilitating the calculations of the reaction extent.

The reaction extent is supposed zero at reactor inlet. Then each reaction extent ξ_i is simply linked to reaction rate with Eq. 1. Dimensionless extent of reaction χ_i is used, which represents the molar flow of reaction i divided par the reference molar flow:

$$\xi_i = r_i \cdot m_{\text{cat}} = F_0 \cdot \chi_i \quad (1)$$

r_i is given by the power law's equations, presented in Eq. 2 and Eq. 3 for Sabatier reaction and Eq. 5 and Eq. 6 for RWGS reaction. It is important to highlight that this model has been established supposing the isothermicity of the catalytic bed.

In the literature we can find several ways of writing a kinetic model of a reaction on solid catalysis [25–28]. The list of parameters will have to be modified according to the model chosen. To test our model, we have chosen the two most commonly used. For our main reaction, Sabatier reaction, we have considered applying the empirical power law

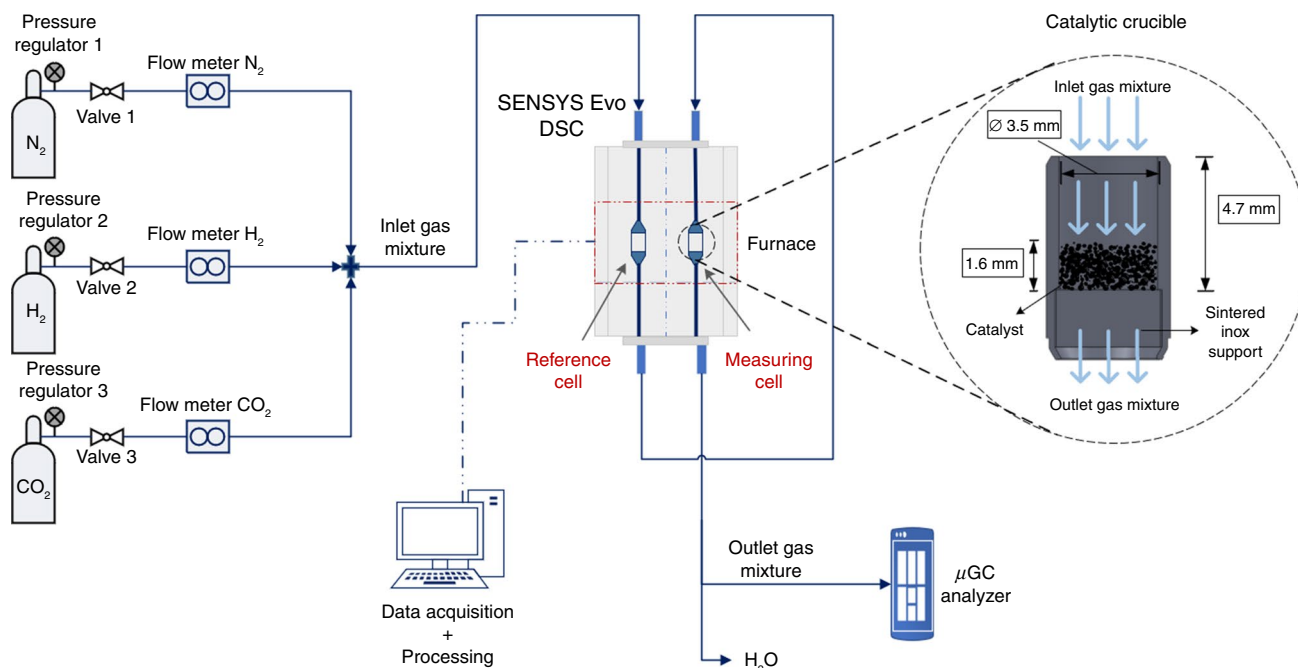


Fig. 1 Schematic representation of the experimental installation

equations proposed by Lunde and Kester [29] (PL-1) as shown in Eq. 2, and the power law equations considering the reaction orders of hydrogen and carbon dioxide as Koschany et al. [18] (PL-2) as shown in Eq. 3. The equilibrium constant expression used in both power laws was the empirical expression as a function of temperature developed by Lunde and Kester [29] as shown in Eq. 4.

$$\text{PL} - 1r_1 = k_{\infty,1} \cdot \exp\left(\frac{-Ea_1}{R \cdot T}\right) \cdot \left(p_{\text{CO}_2}^{n_1} \cdot p_{\text{H}_2}^{4n_1} - \frac{p_{\text{CH}_4}^{n_1} \cdot p_{\text{H}_2\text{O}}^{2n_1}}{K_{\text{eq}_1}^{n_1}} \right) \quad (2)$$

$$\text{PL} - 2r_1 = k_{\infty,1} \cdot \exp\left(\frac{-Ea_1}{R \cdot T}\right) \cdot p_{\text{CO}_2}^{o_1} \cdot p_{\text{H}_2}^{o_2} \cdot \left(1 - \frac{p_{\text{CH}_4} \cdot p_{\text{H}_2\text{O}}^2}{K_{\text{eq}_1} \cdot p_{\text{CO}_2} \cdot p_{\text{H}_2}} \right) \quad (3)$$

$$K_{\text{eq}_1}(T) = \exp\left[\left(\frac{1}{1.987}\right)\left(\frac{56000}{T^2} + \frac{34633}{T} - 16.4 \ln T + 0.00557T\right) + 33.165\right] \quad (4)$$

For the secondary reaction, the reverse water gas shift (RWGS), we have considered applying Lunde and Kester's power law to this reaction as shown in Eq. 5, and a similar power law considering the reaction orders of hydrogen and carbon dioxide for this reaction used by [20] as shown in Eq. 6. The equilibrium constant expression used in both power laws was taken from the equilibrium equation of the water gas shift (WGS) reaction as function of temperature, developed by Twigg [30] considering that, $K_{\text{eq}_2}(T) = \frac{1}{K_{\text{eqRWGS}}(T)}$ as shown in Eq. 7 below.

$$\text{PL} - 1r_2 = k_{\infty,2} \cdot \exp\left(\frac{-Ea_2}{R \cdot T}\right) \cdot \left(p_{\text{CO}_2}^{n_2} \cdot p_{\text{H}_2}^{n_2} - \frac{p_{\text{CO}}^{n_2} \cdot p_{\text{H}_2\text{O}}^{n_2}}{K_{\text{eq}_1}^{n_2}} \right) \quad (5)$$

$$\text{PL} - 2r_2 = k_{\infty,2} \cdot \exp\left(\frac{-Ea_2}{R \cdot T}\right) \cdot p_{\text{CO}_2}^{o_3} \cdot p_{\text{H}_2}^{o_4} \cdot \left(1 - \frac{p_{\text{CO}} \cdot p_{\text{H}_2\text{O}}}{K_{\text{eq}_2} \cdot p_{\text{CO}_2} \cdot p_{\text{H}_2}} \right) \quad (6)$$

$$\frac{1}{\ln(K_{\text{eq}_2}(T))} = \frac{5693.5}{T} + 1.077 \ln(T) + 5.44 \cdot 10^{-4} - 1.125 \cdot 10^{-7} T^2 - \frac{49170}{T^2} - 13.148 \quad (7)$$

Mass balance

Flow rates

Our model considers a CSTR, therefore, temperature T and pressure P at outlet are considered the same as inside the

reactor. The molar flow rate of CO₂ at the inlet was chosen as reference molar flow rate F₀. Molar flow rates ratios are given by Eq. 8. Considering that extent is zero at reactor inlet, molar flow rates at the outlet of the reactor are given in Eqs. 9 and 10 respectively for each species j and in total.

$$Y_j = \frac{F_j^{\text{in}}}{F_0} \quad (8)$$

$$F_j^{\text{out}} = F_0 \cdot \left(Y_j + \sum_i v_{i,j} \cdot \chi_i \right) \quad (9)$$

$$F^{\text{out}} = F_0 \cdot \left(\sum_j Y_j + \sum_i \chi_i \cdot \sum_j v_{i,j} \right) \quad (10)$$

The chemical expansion is calculated by Eq. 11. It considers the non-conservation of the number of molecules in each reaction i.

$$\alpha_i = \sum_j v_{i,j} \quad (11)$$

Partial pressures

Partial pressures of each constituent at the outlet can be calculated with Eq. 12.

$$p_j = P \cdot \frac{F_j^{\text{out}}}{F^{\text{out}}} \quad (12)$$

Substituting the molar flows by Eqs. 9 and 10, we can obtain the expression of the partial pressure as a function of the reaction extent given in Eq. 13.

$$p_j = P \cdot \frac{Y_j + \sum_i v_{i,j} \cdot \chi_i}{\sum_j Y_j + \sum_i \alpha_i \cdot \chi_i} \quad (13)$$

Power balance

According to the instantaneous energy balance in the steady state and isothermal mode in a continuous flow reactor, the total heat flow produced by the reaction can be written as function of the extent of the reaction as shown in Eq. 14, where ΔH_i is the enthalpy of reaction in $\text{J}\cdot\text{mol}^{-1}_{\text{CO}_2}$, and χ_i reaction extent for each reaction i .

$$\dot{q} = - \sum_i \chi_i \cdot F_0 \cdot \Delta H_i \tag{14}$$

Heat and mass transfer limitation study and operating conditions

To propose a rate expression that describes intrinsic reaction kinetics and that is suitable for reactors design calculations, operating conditions should be selected to respect isothermicity in the catalytic bed. For this reason, we carried out a theoretical study based on different heat transfer limitation criteria: Prater criteria to obtain the dimensionless maximum temperature rise in the catalyst [31], Mears criteria for the evaluation of the absence of external heat transfer limitation [32], and Anderson criteria for the evaluation of the internal resistance to heat transfer [33]. The equations of these criteria can be found in the supporting information.

For the evaluations of these criteria, a large range of stoichiometric and non-stoichiometric operating conditions with different ratios of reactant H_2/CO_2 and N_2 as carrier gas in the inlet flow at different isothermal conditions in an interval of temperature between 573 and 673 K with an increase of 10 K have been selected.

The furnace temperature at highest measured heat flow was 673 K, thus we carried out the evaluation of heat transfer limitations at this temperature to obtain the worst value for each criterion. We have considered that only our main reaction occurred and the measured heat flow was generated by this reaction. Table 1 shows the results of this evaluation and the operating conditions that will be used for the kinetic study at different temperatures. We can see that those selected operating conditions respect all heat transfer criteria that allows us to ensure the isothermicity of the catalytic bed during the reaction.

To confirm the homogeneity of the composition, mass transfer limitation was evaluated using two important criteria, Weisz-Prater criteria for the evaluation of the absence of significant intraphase diffusion effects [34], and Mears criteria for the evaluation of the absence of external mass transfer limitation [35]. The equations of these criteria can be found in the supporting information. Table 2 shows the results of this evaluation for each operating condition. Satisfaction of these criteria demonstrates that interphase and intraphase mass transfer is not significantly affecting the measured rate.

Estimation of kinetic parameters in continuous DSC

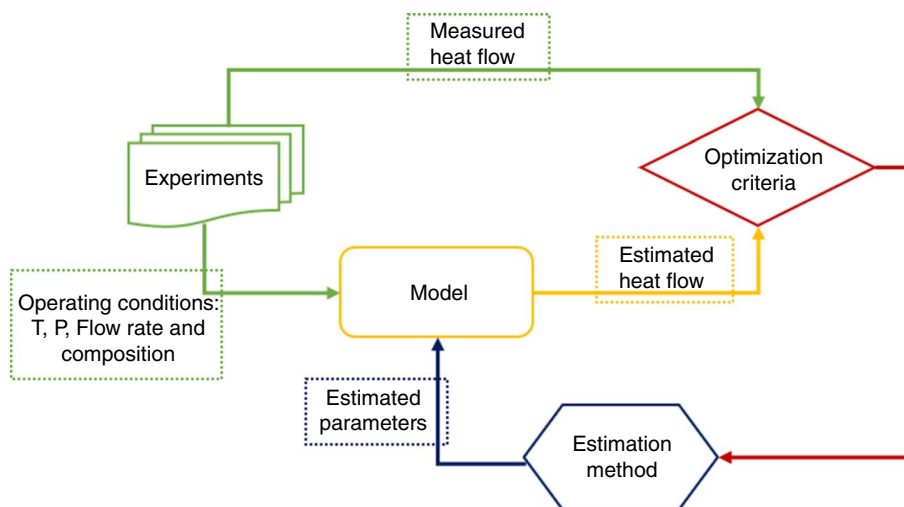
The approach, described in Fig. 2, consists in a classical parameter estimation method based on the comparison of the estimated heat flow from the kinetic model to the measured one. The optimization criteria indicates the accuracy of the set of kinetic parameters used; the lower the criteria, the better the model will represent the experiments.

Table 1 Operating conditions and heat transfer limitation results for a furnace temperature of 673 K and catalytic powder with diameter < 50 μm

H_2/CO_2	Operating conditions				Heat transfer imitation criteria		
	$F_{\text{mix}}/\text{mol h}^{-1}$	y_{N_2}	y_{H_2}	y_{CO_2}	Anderson limit < 0.75	Mears limit < 0.15	Prater (K) limit < 5 K
4	0.25	50.0%	40.0%	10.0%	6×10^{-4}	0.016	2.1
	0.50				5×10^{-4}	0.014	2.1
	0.25	30.0%	56.0%	14.0%	9×10^{-4}	0.020	2.9
	0.50				7×10^{-4}	0.015	2.9
7	0.25	10.0%	72.0%	18.0%	8×10^{-4}	0.015	3.7
	0.25	50.0%	43.7%	6.3%	6×10^{-4}	0.012	1.3
	0.50				4×10^{-4}	0.009	1.3
	0.25	30.0%	61.3%	8.7%	9×10^{-4}	0.015	1.8
3	0.50				6×10^{-4}	0.011	1.8
	0.25	10.0%	78.7%	11.3%	8×10^{-4}	0.012	2.3
	0.25	50.0%	37.5%	12.5%	6×10^{-4}	0.017	2.0
	0.50				4×10^{-4}	0.012	2.0
3	0.25	30.0%	52.5%	17.5%	7×10^{-4}	0.018	2.7
	0.50				6×10^{-4}	0.015	2.7
	0.25	10.0%	67.5%	22.5%	9×10^{-4}	0.020	3.5

Table 2 Operating conditions and mass transfer limitation results for a furnace temperature of 673 K and catalytic powder with diameter <math>< 50 \mu\text{m}</math>

H_2/CO_2	Operating conditions				Mass transfer imitation criteria	
	$\dot{F}_{\text{mix}} / \text{mol h}^{-1}$	y_{N_2}	y_{H_2}	y_{CO_2}	Weisz–Prater limit ≤ 1	Mears limit < 0.15
4	0.25	50.0%	40.0%	10.0%	0.10	0.016
	0.50				0.11	0.013
	0.25	30.0%	56.0%	14.0%	0.11	0.032
	0.50				0.09	0.023
	0.25	10.0%	72.0%	18.0%	0.08	0.034
7	0.25	50.0%	43.7%	6.3%	0.16	0.009
	0.50				0.17	0.007
	0.25	30.0%	61.3%	8.7%	0.18	0.018
	0.50				0.15	0.013
	0.25	10.0%	78.7%	11.3%	0.16	0.022
3	0.25	50.0%	37.5%	12.5%	0.08	0.019
	0.50				0.06	0.013
	0.25	30.0%	52.5%	17.5%	0.07	0.031
	0.50				0.06	0.026
	0.25	10.0%	67.5%	22.5%	0.07	0.050

Fig. 2 Principle of estimation of kinetic parameters

Estimation method

Due to high number of parameters to estimate (8 parameters: pre-exponential factor, activation energy and reaction orders for each reaction), a locally convergent estimation method would need to be initialized with a set of values of the parameters to be estimated not too far from the solution. To overcome this defect, especially when the order of magnitude of the solution is difficult to estimate a priori, it may be advantageous to turn to a globally convergent method. These methods will simultaneously handle several sets of values of the parameters to be estimated.

Genetic Algorithms are estimation methods which are independent of the starting point and able to search in

the entire space. The estimation method based on genetic algorithm is an advanced method for kinetic parameters determination [36]. This method combines a genetic algorithm for initial parameters generation with a local convergence method used for parameters optimization [37]. We have developed a program using Scilab for the estimation parameters based on genetic algorithm. The objective of this program is to find the value of χ_i in Eq. 1 that makes this algebraic equation for a CSTR equal to zero using the Powell’s hybrid algorithm method (fsolve Scilab) for the solution. We used the power law equations (Sect. “Hypothesis”) and the mass balance equations (Sect. “Mass balance”) expressed as a function of χ_i for this purpose. Then as optimization function we have used “optim_ga”

to minimize the criterion shown in Eq. 15 where the heat flow \dot{q} is calculated as function of χ_i as show with Eq. 14 to finally estimate the kinetic parameters.

The criterion will indicate to the estimation method the accuracy of the set of kinetic parameters to be estimated. In our study, we have used a criterion expression as a function of the measured heat flow release by the reaction, considering NE experiments.

$$f_{\dot{q}} = \sum_{k=1}^{NE} \frac{|\dot{q}_k^{\text{calc}} - \dot{q}_k^{\text{exp}}|}{\dot{q}_k^{\text{exp}}} \quad (15)$$

Results and discussion

Heat flow measurements and accuracy in the DSC device

Accuracy of heat flow measurements

To validate that the DSC measurements correspond to heat flow released by the reaction, we selected one experiment and analyzed the outlet gases continuously using a μGC , obtaining the concentration of each product gas in the outlet. Thanks to these concentration data, we were able to calculate the extent of each reaction and then calculate the μGC heat flow using Eq. 14. This allows us to make a comparison between the heat flow measured by the DSC and the μGC heat flow as show in Fig. 3. We can see that most of measured heat flow points have less than 5% of deviation from the μGC one. The coefficient of determination R^2 in the linear regression is 0.993 which indicates

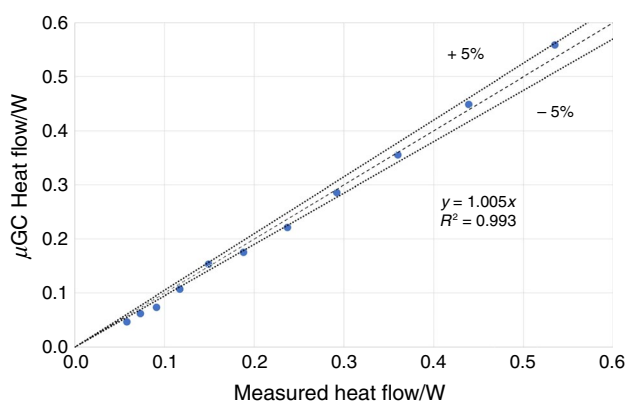


Fig. 3 Parity plot comparing the measured heat flow against μGC heat flow calculated with the values of the reaction extent given by the μGC analysis. The operation condition was Ratio $\text{H}_2/\text{CO}_2=3$, $y_{\text{N}_2}=0.3$ and $\dot{F}_{\text{mix}}=0.5 \text{ mol h}^{-1}$

that the measured heat flow is very close to the analytical values confirming the accuracy of the measurements.

Evolution of measured heat flow versus temperature

Figure 4 shows some results of the measured heat flow by the DSC as function of temperature in the range 573–673 K; the other results can be found in the supporting information. Globally, in Fig. 4 we can see the effect of temperature for all operating conditions. As the temperature increases the measured heat flow increases independently of the gas mixture at the inlet, this is because the main reaction is exothermic and is favored at high temperatures. Figure 4a shows the effect of N_2 dilution on the inlet gas mixture. We can see that the lower the dilution of N_2 , the higher the heat release during the reaction. This is because there is a higher conversion in the reaction because there is more reactant in the mixture. Figure 4b shows the effect of the total molar flow of the inlet for the same dilution with 30% N_2 . We can see that the lower the temperature, the lower the heat released during the reaction. This is because there is less reactant flow. Figure 4c shows the effect of the reagent ratio H_2/CO_2 for the same gas mixture flow at the inlet $\dot{F}_{\text{mix}}=0.25 \text{ mol h}^{-1}$ and y_{N_2} . We can see that the heat flow for a ratio of $\text{H}_2/\text{CO}_2=3$ is slightly lower than for the other two ratios $\text{H}_2/\text{CO}_2=4$ and 7 because there is a lower conversion in the reaction since the mixture does not have the stoichiometry that favors the exothermic main reaction.

Parameters estimation results

The estimation of the kinetic parameters for both power law found in Eqs. 2 and 3 for Sabatier reaction and Eqs. 5 and 6 for RWGS reaction, was carried out considering the 165 experimental points obtained from the different operating conditions with different ratios of reactant H_2/CO_2 and N_2 as carrier gas as show in Table 1 and 2 and the variation furnace temperature in an interval between 573 and 673 K with an increase of 10 K.

We made a comparison with some parameter estimated by other authors for our main reaction, we also compared the value of the Arrhenius constant $k_{i,T_{\text{ref}}} = k_{\infty,i} \cdot \exp\left(\frac{-Ea_i}{R \cdot T_{\text{ref}}}\right)$ at a reference temperature of 610 K for each reaction since the values of $k_{\infty,i}$ are not comparable. Uncertainties of these parameters were assessed considering 5 parameters estimations in which the genetic algorithm converges close to the same value of the optimization criterion.

Tables 3 and 4 show the parameter estimation results with PL-1 and PL-2 respectively. We can see that the order of magnitude of $k_{i,610\text{K}}$ results are within the interval of the other authors. Although there are still some differences in the results, this may be related to probably not using the

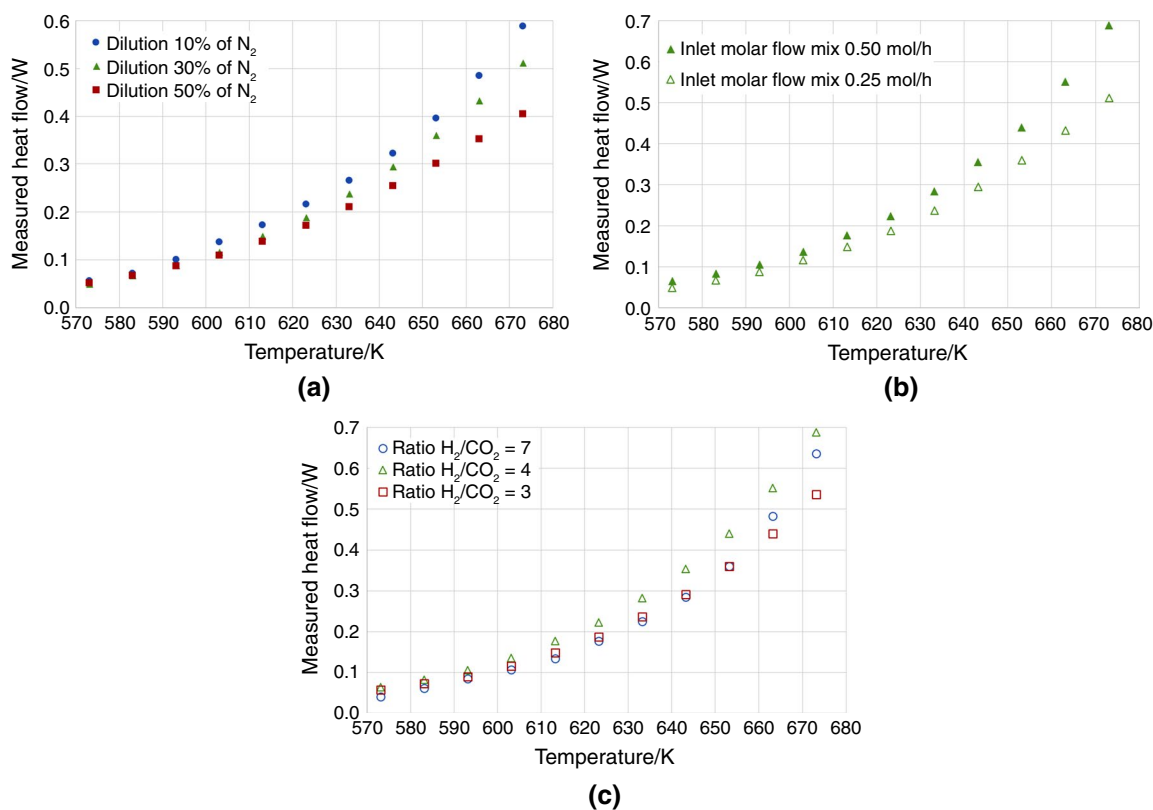


Fig. 4 Measured heat flow vs temperature. **a** Operating conditions with different dilution of N₂ and ratio H₂/CO₂=4 and F_{mix}=0.25 mol h⁻¹; **b** operating conditions with different inlet

molar flow mix with ratio H₂/CO₂=4 and y_{N₂}=0.3; **c** operating conditions with different ratios of H₂/CO₂ and molar flow inlet F_{mix}=0.5 mol h⁻¹ and y_{N₂}=0.3

same operating conditions, type of catalyst (same amount, same manufacturer or metal composition etc.).

In our results, the difference between the values of the activation energy of the Sabatier reaction (R1) and that of RWGS (R2) is normal because the reaction (R2) starts to take place at higher temperatures than R1 and therefore needs a higher activation energy.

Figure 5 provides the parity plot of the comparison of the estimated heat flow with PL-1 and PL-2 versus the measured heat flow for all the experiments, and a visualization of the deviation of a visualization of the deviation of both models from the experimental data. In both graph R² and the slope of the linear regression are approximately 1. These results indicate a good prediction of the heat flow by the two models.

Figure 5a shows the results of the PL-1. The points are less dispersed but have a lower parity for measured heat flows higher than 0.5 W. Figure 5b shows the results of the PL-2. The points are more dispersed but they maintain the parity points.

Figure 6 shows the comparison between the reaction extent obtained from μGC analysis and the estimated reaction extent of both reactions for one experiment. Figure 6a shows the results of the estimation using PL-1. The estimated extent for reaction 1 achieves a good fit with the μGC values but we can see a variation of results from temperatures 643 to 673 K for the estimated extent for reaction 2. Figure 6b shows the results of the estimation using PL-2. The estimated reaction extent gets close to the analyzed ones, validating our estimation results for this model.

Table 3 Parameters estimation results with PL-1

Parameters	Sabatier reaction				Reverse water gas shift reaction			
	$k_{\infty 1}$ mol g ⁻¹ s ⁻¹ bar ⁻⁵ⁿ¹	E_{a1} kJ mol ⁻¹	k_{1610K} mol g ⁻¹ s ⁻¹ bar ⁻⁵ⁿ¹	n_1	$k_{\infty 2}$ mol g ⁻¹ s ⁻¹ bar ⁻⁵ⁿ²	E_{a2} kJ mol ⁻¹	k_{2610K} mol g ⁻¹ s ⁻¹ bar ⁻⁵ⁿ²	n_2
<i>This work</i>	<i>(5.26 ± 0.64) × 10³</i>	<i>89.15 ± 0.67</i>	<i>(1.22 ± 0.02) × 10⁻⁴</i>	<i>0.10 ± 0.002</i>	<i>(19.2 ± 0.03) × 10⁴</i>	<i>109.63 ± 9.25</i>	<i>(7.77 ± 0.53) × 10⁻⁵</i>	<i>0.79 ± 0.19</i>
[17]	(1.45 ± 0.07) × 10 ³	73 ± 0.4	(8.13 ± 0.39) × 10 ⁻⁴	0.35 ± 0.1	-	-	-	-
[29]	18.30 ± 0.06	68 ± 0.3	(2.75 ± 0.18) × 10 ⁻⁵	0.14 ± 0.001	-	-	-	-
[38]	9.40 ± 0.01	65 ± 0.2	(2.55 ± 0.22) × 10 ⁻⁵	0.076 ± 0.001	-	-	-	-
<i>This work</i>	<i>(5.26 ± 0.64) × 10³</i>	<i>89.15 ± 0.67</i>	<i>(1.22 ± 0.02) × 10⁻⁴</i>	<i>0.10 ± 0.002</i>	<i>(19.2 ± 0.03) × 10⁴</i>	<i>109.63 ± 9.25</i>	<i>(7.77 ± 0.53) × 10⁻⁵</i>	<i>0.79 ± 0.19</i>
[17]	(1.45 ± 0.07) × 10 ³	73 ± 0.4	(8.13 ± 0.39) × 10 ⁻⁴	0.35 ± 0.1	-	-	-	-
[29]	18.30 ± 0.06	68 ± 0.3	(2.75 ± 0.18) × 10 ⁻⁵	0.14 ± 0.001	-	-	-	-
[38]	9.40 ± 0.01	65 ± 0.2	(2.55 ± 0.22) × 10 ⁻⁵	0.076 ± 0.001	-	-	-	-
<i>This work</i>	<i>(5.26 ± 0.64) × 10³</i>	<i>89.15 ± 0.67</i>	<i>(1.22 ± 0.02) × 10⁻⁴</i>	<i>0.10 ± 0.002</i>	<i>(19.2 ± 0.03) × 10⁴</i>	<i>109.63 ± 9.25</i>	<i>(7.77 ± 0.53) × 10⁻⁵</i>	<i>0.79 ± 0.19</i>
[17]	(1.45 ± 0.07) × 10 ³	73 ± 0.4	(8.13 ± 0.39) × 10 ⁻⁴	0.35 ± 0.1	-	-	-	-
[29]	18.30 ± 0.06	68 ± 0.3	(2.75 ± 0.18) × 10 ⁻⁵	0.14 ± 0.001	-	-	-	-
[38]	9.40 ± 0.01	65 ± 0.2	(2.55 ± 0.22) × 10 ⁻⁵	0.076 ± 0.001	-	-	-	-

Italics indicate that the values are the results of this work

Table 4 Parameters estimation results with PL-2 (Italics indicate our results)

Parameters	Sabatier reaction				Reverse water gas shift reaction					
	$k_{\infty 1}$ mol g ⁻¹ s ⁻¹ bar ⁻⁽⁰¹⁺⁰²⁾	E_{a1} kJ mol ⁻¹	k_{1610} mol g ⁻¹ s ⁻¹ bar ⁻⁽⁰¹⁺⁰²⁾	O_1	O_2	$k_{\infty 2}$ mol g ⁻¹ s ⁻¹ bar ⁻⁽⁰³⁺⁰⁴⁾	E_{a2} kJ mol ⁻¹	k_{2610} mol g ⁻¹ s ⁻¹ bar ⁻⁽⁰³⁺⁰⁴⁾	O_3	O_4
<i>This work</i>	<i>(1.01 ± 0.29) × 10³</i>	<i>80.41 ± 0.95</i>	<i>(1.31 ± 0.16) × 10⁻⁴</i>	<i>0.20 ± 0.02</i>	<i>0.40 ± 0.04</i>	<i>1.01 × 10⁶</i>	<i>116.38 ± 8.65</i>	<i>(1.10 ± 0.95) × 10⁻⁴</i>	<i>0.55 ± 0.10</i>	<i>0.59 ± 0.18</i>
[18]	(4.13 ± 0.19) × 10 ⁴	93.6 ± 2.5	(3.99 ± 1.51) × 10 ⁻⁴	0.31 ± 0.02	0.16 ± 0.02	-	-	-	-	-
[20]	-	-	-	-	-	707	85.3	3.51 × 10 ⁻⁵	0.2	0.03
<i>This work</i>	<i>(1.01 ± 0.29) × 10³</i>	<i>80.41 ± 0.95</i>	<i>(1.31 ± 0.16) × 10⁻⁴</i>	<i>0.20 ± 0.02</i>	<i>0.40 ± 0.04</i>	<i>1.01 × 10⁶</i>	<i>116.38 ± 8.65</i>	<i>(1.10 ± 0.95) × 10⁻⁴</i>	<i>0.55 ± 0.10</i>	<i>0.59 ± 0.18</i>
[18]	(4.13 ± 0.19) × 10 ⁴	93.6 ± 2.5	(3.99 ± 1.51) × 10 ⁻⁴	0.31 ± 0.02	0.16 ± 0.02	-	-	-	-	-
[20]	-	-	-	-	-	707	85.3	3.51 × 10 ⁻⁵	0.2	0.03
<i>This work</i>	<i>(1.01 ± 0.29) × 10³</i>	<i>80.41 ± 0.95</i>	<i>(1.31 ± 0.16) × 10⁻⁴</i>	<i>0.20 ± 0.02</i>	<i>0.40 ± 0.04</i>	<i>1.01 × 10⁶</i>	<i>116.38 ± 8.65</i>	<i>(1.10 ± 0.95) × 10⁻⁴</i>	<i>0.55 ± 0.10</i>	<i>0.59 ± 0.18</i>
[18]	(4.13 ± 0.19) × 10 ⁴	93.6 ± 2.5	(3.99 ± 1.51) × 10 ⁻⁴	0.31 ± 0.02	0.16 ± 0.02	-	-	-	-	-
[20]	-	-	-	-	-	707	85.3	3.51 × 10 ⁻⁵	0.2	0.03

Italics indicate that the values are the results of this work

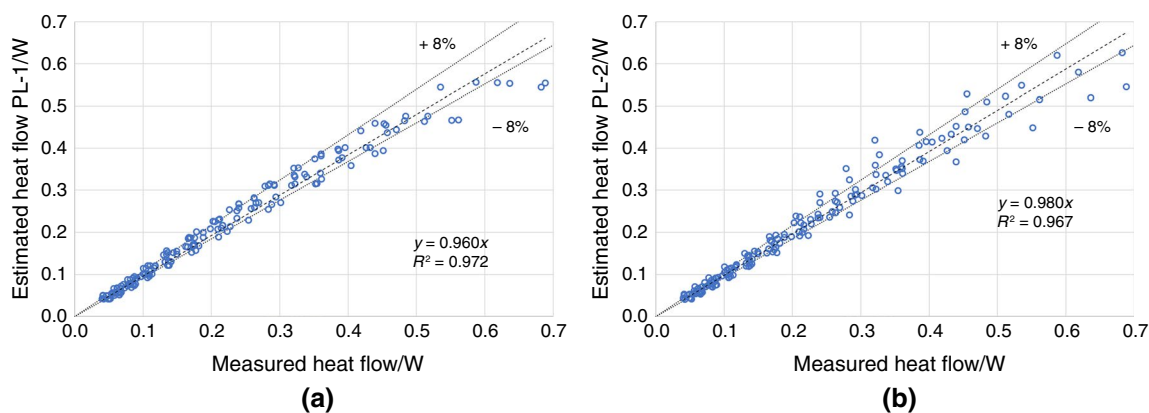
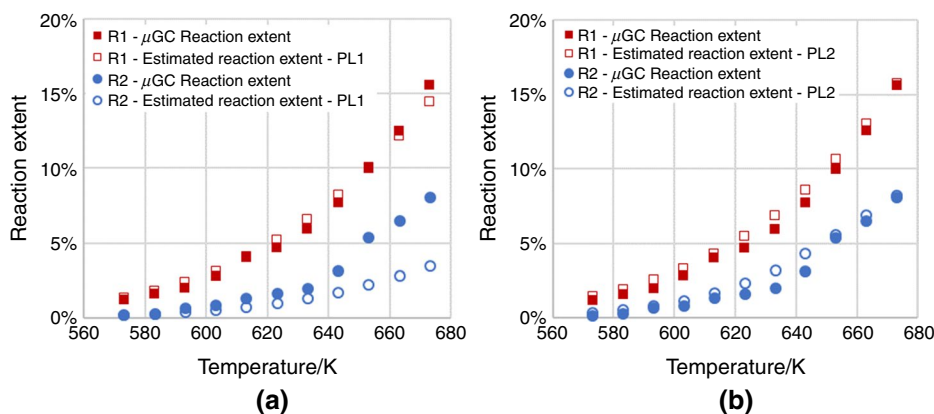


Fig. 5 Parity plot comparing the estimated heat flow and the measured heat flow by DSC device for all operating conditions and temperatures between 573 and 673 K for **a** PL-1, **b** PL-2

Fig. 6 Comparison between the estimated reaction extent and the μ GC reaction extent reaction calculated with the concentrations given by the μ GC for both reactions. The operation condition was ratio $H_2/CO_2 = 3$, $y_{N_2} = 0.3$ and $F_{mix} = 0.5 \text{ mol h}^{-1}$. For **a** PL-1, **b** PL-2



Conclusions

We have presented an isothermal model based on a CSTR for the estimation of kinetic parameters in continuous flow. For the estimation of these parameters, we have used a genetic algorithm considering the relative absolute difference between the measured heat flow and the calculated one as an optimization criterion. Our approach involved the use of a DSC in continuous flow with a crucible containing a catalytic bed for the measurement of heat flow during the chemical reaction. To ensure the isothermicity of the catalytic bed in DSC and to determine the intrinsic kinetics of the reaction, it is necessary to overcome the internal and external limitations of heat and mass transfer in the catalytic bed. It is important to use operating conditions where the heat flow is high enough to be measured accurately, but not too high so that the temperature in the bed does not increase. Continuous flow DSC provides a high level of sensitivity and accuracy for heat flow measurement, allowing the detection of small changes in heat flow associated with reactions. This is a simple and fast

method that uses a small sample volume. Our results demonstrate the effectiveness of this methodology for the estimation of kinetic parameters in the hydrogenation of CO_2 in methane. For the study of operating conditions with high heat flows, it is necessary to change from isothermal to non-isothermal model to consider the temperature change in the bed.

Supplementary Information The online version contains supplementary material available at <https://doi.org/10.1007/s10973-023-12849-z>.

Acknowledgements For the financial and analytical part, the authors thank the Ministry of High Education, Science and Technology of Dominican Republic (MESCYT), University of Rouen Normandy, National Institute of Applied Sciences (INSA) Rouen Normandy and Chemical Process Safety Laboratory (LSPC).

Author contributions All authors contributed to the study conception and design. Material preparation, data collection and analysis were performed by all authors. The first draft of the manuscript was written by Yamily Mateo Rosado and all authors commented on previous versions of the manuscript. All authors read and approved the final manuscript.

Funding The authors did not receive support from any organization for the submitted work.

References

- Hackney AC. Measurement techniques for energy expenditure. In: Exercise, sport, and bioanalytical chemistry. Elsevier; 2016. p. 33–42. <https://doi.org/10.1016/B978-0-12-809206-4.00013-5>.
- Auroux Éd A. Calorimetry and thermal methods in catalysis. In: Series in materials science, vol. 154. Berlin: Springer; 2013. <https://doi.org/10.1007/978-3-642-11954-5>.
- Frede TA, Maier MC, Kockmann N, Gruber-Woelfler H. Advances in continuous flow calorimetry. *Org Process Res Dev*. 2022;26(2):267–77. <https://doi.org/10.1021/acs.oprd.1c00437>.
- Gesthuisen R, Krämer S, Niggemann G, Leiza JR, Asua JM. Determining the best reaction calorimetry technique: theoretical development. *Comput Chem Eng*. 2005;29(2):349–65. <https://doi.org/10.1016/j.compchemeng.2004.10.009>.
- Hemminger W, Höhne G, Hemminger W. Calorimetry—fundamentals and practice. Weinheim: Verl; 1984.
- Zogg A, Stoessel F, Fischer U, Hungerbühler K. Isothermal reaction calorimetry as a tool for kinetic analysis. *Thermochim Acta*. 2004;419(1–2):1–17. <https://doi.org/10.1016/j.tca.2004.01.015>.
- Ebeid E-ZM, Zakaria MB. State of the art and definitions of various thermal analysis techniques. In: Thermal Analysis. Elsevier; 2021. p. 1–39.
- Krell T. Microcalorimetry: a response to challenges in modern biotechnology. *Microb Biotechnol*. 2008;1(2):126–36. <https://doi.org/10.1111/j.1751-7915.2007.00013x>.
- Höhne G, Hemminger W, Flammersheim H-J, Hemminger WF, Flammersheim H-J. Differential Scanning Calorimetry. 2 enlarged. Berlin: Springer; 2010.
- Harvey J-P, Saadatkah N, Dumont-Vandewinkel G, Ackermann SLG, Patience GS. Experimental methods in chemical engineering: differential scanning calorimetry-DSC. *Can J Chem Eng*. 2018;96(12):2518–25. <https://doi.org/10.1002/cjce.23346>.
- Drzeżdżon J, Jacewicz D, Sielicka A, Chmurzyński L. Characterization of polymers based on differential scanning calorimetry based techniques. *TrAC Trends Anal Chem*. 2019;110:51–6. <https://doi.org/10.1016/j.trac.2018.10.037>.
- Clas S-D, Dalton CR, Hancock BC. Differential scanning calorimetry: applications in drug development. *Pharm Sci Technol Today*. 1999;2(8):311–20. [https://doi.org/10.1016/S1461-5347\(99\)00181-9](https://doi.org/10.1016/S1461-5347(99)00181-9).
- Leyva-Porras C, et al. Application of differential scanning calorimetry (DSC) and modulated differential scanning calorimetry (MDSC) in food and drug industries. *Polymers*. 2019;12(1):5. <https://doi.org/10.3390/polym12010005>.
- Pagano RL, Calado VMA, Tavares FW, Biscaia EC. Cure kinetic parameter estimation of thermosetting resins with isothermal data by using particle swarm optimization. *Eur Polym J*. 2008;44(8):2678–86. <https://doi.org/10.1016/j.eurpolymj.2008.05.017>.
- Pagano RL, Calado VMA, Tavares FW, Biscaia EC. Parameter estimation of kinetic cure using DSC non-isothermal data. *J Therm Anal Calorim*. 2011;103(2):495–9. <https://doi.org/10.1007/s10973-010-0984-5>.
- Alrafei B, Polaert I, Ledoux A, Azzolina-Jury F. Remarkably stable and efficient Ni and Ni–Co catalysts for CO₂ methanation. *Catal Today*. 2020;346:23–33. <https://doi.org/10.1016/j.cattod.2019.03.026>.
- Alrafei B. Etude catalytique et cinétique de la méthanation du CO en lit fixe et sous plasma micro-ondes Insa Rouen, 2020. [En ligne]. Disponible sur: <https://tel.archives-ouvertes.fr/tel-02924546/document>
- Koschany F, Schlereth D, Hinrichsen O. On the kinetics of the methanation of carbon dioxide on coprecipitated NiAl(O). *Appl Catal B Environ*. 2016;181:504–16. <https://doi.org/10.1016/j.apcatb.2015.07.026>.
- Rönsch S, et al. Review on methanation—from fundamentals to current projects. *Fuel*. 2016;166:276–96. <https://doi.org/10.1016/j.fuel.2015.10.111>.
- Marocco P, et al. CO₂ methanation over Ni/Al hydrotalcite-derived catalyst: experimental characterization and kinetic study. *Fuel*. 2018;225:230–42. <https://doi.org/10.1016/j.fuel.2018.03.137>.
- Khuenpetch A, Choi C, Reubroycharoen P, Norinaga K. Development of a kinetic model for CO₂ methanation over a commercial Ni/SiO₂ catalyst in a differential reactor. *Energy Rep*. 2022;8:224–33. <https://doi.org/10.1016/j.egy.2022.10.194>.
- Al-Ghussain L. Global warming: review on driving forces and mitigation: global warming: review on driving forces and mitigation. *Environ Prog Sust Energy*. 2019;38(1):13–21. <https://doi.org/10.1002/ep.13041>.
- Saeidi S, Amin NAS, Rahimpour MR. Hydrogenation of CO₂ to value-added products—a review and potential future developments. *J CO₂ Util*. 2014;5:66–81. <https://doi.org/10.1016/j.jcou.2013.12.005>.
- Chemlys, Micro GC Fusion Brochure and Specifications [En ligne]. Disponible sur: <https://www.chemlys.com/en/portfolio/micro-gc-fusion-brochure-and-specifications/>
- Choi C, et al. Determination of kinetic parameters for CO₂ methanation (Sabatier Reaction) over Ni/ZrO₂ at a stoichiometric feed-gas composition under elevated pressure. *Energy Fuels*. 2021;35(24):20216–23. <https://doi.org/10.1021/acs.energyfuels.1c01534>.
- Schlereth D, Hinrichsen O. A fixed-bed reactor modeling study on the methanation of CO₂. *Chem Eng Res Des*. 2014;92(4):702–12. <https://doi.org/10.1016/j.cherd.2013.11.014>.
- Ducamp J, Bengaouer A, Baurens P, Fechete I, Turek P, Garin F. Statu quo sur la méthanation du dioxyde de carbone : une revue de la littérature. *C R Chim*. 2018;21(3–4):427–69. <https://doi.org/10.1016/j.crci.2017.07.005>.
- Quezada MJ. Hydrogénation catalytique de CO₂ en méthanol en lit fixe sous chauffage conventionnel et sous plasma à DBD Insa Rouen, 2021. [En ligne]. Disponible sur: <https://tel.archives-ouvertes.fr/tel-03215410/document>
- Lunde P. Rates of methane formation from carbon dioxide and hydrogen over a ruthenium catalyst. *J Catal*. 1973;30(3):423–9. [https://doi.org/10.1016/0021-9517\(73\)90159-0](https://doi.org/10.1016/0021-9517(73)90159-0).
- Twigg MV. Catalyst handbook. 2nd ed. London: Routledge; 1989. p. 1989.
- Villermaux J. *Génie de la réaction chimique: conception et fonctionnement des réacteurs*, 2e éd. rev. et Augm. in Génie des procédés de l'Ecole de Nancy. Paris: Tec et doc, 1993
- Trambouze P, Euzen J-P. Chemical reactors: from design to operation. Institut français du pétrole publications Editions Technip; 2004.
- Davis ME, Davis RJ. Fundamentals of chemical reaction engineering. N.Y Dover Publications; 2012.
- Weisz PB, Prater CD. Interpretation of measurements in experimental catalysis. In: Advances in Catalysis, vol. 6. Elsevier; 1954. p. 143–96. [https://doi.org/10.1016/S0360-0564\(08\)60390-9](https://doi.org/10.1016/S0360-0564(08)60390-9).
- Mears DE. Tests for transport limitations in experimental catalytic reactors. *Ind Eng Chem Proc Des Dev*. 1971;10(4):541–7. <https://doi.org/10.1021/i260040a020>.
- Abdelouahed L, Leveneur S, Vernieres-Hassimi L, Balland L, Taouk B. Comparative investigation for the determination of kinetic parameters for biomass pyrolysis by thermogravimetric analysis. *J Therm Anal Calorim*. 2017;129(2):1201–13. <https://doi.org/10.1007/s10973-017-6212-9>.
- Balland L, Estel L, Cosmao J-M, Mouhab N. A genetic algorithm with decimal coding for the estimation of kinetic and energetic

- parameters. *Chemom Intell Lab Syst.* 2000;50(1):121–35. [https://doi.org/10.1016/S0169-7439\(99\)00057-X](https://doi.org/10.1016/S0169-7439(99)00057-X).
38. Falbo L, Martinelli M, Visconti CG, Lietti L, Bassano C, Deiana P. Kinetics of CO₂ methanation on a Ru-based catalyst at process conditions relevant for power-to-gas applications. *Appl Catal B Environ.* 2018;225:354–63. <https://doi.org/10.1016/j.apcatb.2017.11.066>.

Springer Nature or its licensor (e.g. a society or other partner) holds exclusive rights to this article under a publishing agreement with the author(s) or other rightsholder(s); author self-archiving of the accepted manuscript version of this article is solely governed by the terms of such publishing agreement and applicable law.

Publisher's Note Springer Nature remains neutral with regard to jurisdictional claims in published maps and institutional affiliations.